Research Square

Preprints are preliminary reports that have not undergone peer review.
They should not be considered conclusive, used to inform clinical practice,
or referenced by the media as validated information.

Efficient Time–Frequency Representations via the Quadratic-Phase Hilbert Transform

MUSADIQ SHAHEEN

msuok21@gmail.com

University of Kashmir

FIRDOUS A. SHAH

University of Kashmir

Research Article

Keywords: Quadratic-phase Fourier transform, quadratic-phase Hilbert transform, short-time transform, time–frequency analysis, analytic signal, chirp, energy concentration, multi-resolution

Posted Date: September 3rd, 2026

DOI: https://doi.org/10.21203/rs.3.rs-10308998/v1

License: This work is licensed under a Creative Commons Attribution 4.0 International License.
Read Full License

Additional Declarations: No competing interests reported.

EFFICIENT TIME–FREQUENCY REPRESENTATIONS VIA THE QUADRATIC-PHASE HILBERT TRANSFORM

MUSADIQ SHAHEEN AND FIRDOUS A. SHAH

Abstract. Among the class of generalized Fourier transforms, the quadratic-phase Fourier transform (QPFT) is of particular significance as it unifies several prominent integral transforms, such as the Fourier, fractional Fourier, linear-canonical and special-affine Fourier transforms into a single transform endowed with a five-parameter quadratic kernel. Based on such a quadratic kernel, the recently introduced quadratic-phase Hilbert transform (QPHT) extends analytic-signal theory to this generalized domain. Nonetheless, both QPFT and QPHT cannot resolve the temporal evolution of a non-stationary spectrum as the underlying kernels act as global operators. As such it is of significant interest to inculcate localization features into QPFT and QPHT by localizing the quadratic kernel via a window function, which the main motive of this paper. In this direction, we propose the short-time quadratic-phase Fourier transform (ST-QPFT), and its frequency-domain window-size-fixed multi-resolution variant (MR-ST-QPFT), adapted from the STFT-FD construction of Mateo and Talavera [15]. A single structural identity the chirp-reduction lemma reduces every ST-QPFT to an ordinary short-time Fourier transform of a chirp-demodulated signal evaluated on a rescaled frequency axis, and from it we derive boundedness, an energy (Parseval) relation with an explicit factor B^{-1}, an inversion formula, and covariance laws exhibiting the time–frequency shear induced by the quadratic phase. We further clarify the analytic-signal construction by showing that the QPHT is exactly a chirp-conjugated classical Hilbert transform, prove that the associated quadratic-phase analytic signal has a one-sided QPFT spectrum, and define a quadratic-phase Hilbert spectrum through the resulting instantaneous amplitude and frequency. The proposed theory of these novel transforms is substantially endorsed with numerical simulations.

1. Introduction

Time-frequency analysis seeks representations of a signal that simultaneously expose its temporal and spectral structure. For stationary signals the Fourier transform is sufficient, but the overwhelming majority of signals encountered in communications, radar, sonar, seismology and biomedicine are non-stationary: their spectral content evolves with time. The classical device for tracking this evolution is the short-time Fourier transform (STFT),in which the signal is multiplied by a sliding window and Fourier analyzed; its squared modulus, the spectrogram, remains the workhorse of applied time-frequency analysis [1, 2, 3].The STFT is, however, based on the standard Fourier basis of pure harmonics and is therefore poorly matched to signals whose instantaneous frequency varies rapidly, the prototypical example being the linear frequency modulated chirp:the spectrogram of a chirp is an extended diagonal ridge rather than a sharply localized curve, and the time-frequency resolution is fundamentally limited by the fixed window.

A productive response has been to replace the Fourier kernel by a more flexible family. The fractional Fourier transform [4, 5], the linear canonical transform [6] and the special-affine Fourier transform [7] progressively enlarge the class of admissible kernels. The quadratic-phase Fourier transform (QPFT), introduced by Saitoh and developed by Castro and collaborators [9, 10, 8], subsumes all of these through a five parameter quadratic chirp kernel $\exp\{-\mathrm{i}(At^2+Bt\omega+C\omega^2+Dt+E\omega)\}$.Recent work has developed a rich harmonic-analytic theory for this transform, including convolution structures, [13], wave-packet transforms [12], uncertainty principles and pseudo-differential calculus [14].

1991 *Mathematics Subject Classification.* 42A38, 42B10, 42A85, 94A12, 65T99.

Key words and phrases. Quadratic-phase Fourier transform; quadratic-phase Hilbert transform; short-time transform; time–frequency analysis; analytic signal; chirp; energy concentration; multi-resolution.

Closing a visible gap, Srivastava, Shah, Qadri, Lone and Gojree [11] introduced the quadratic-phase Hilbert transform (QPHT), established its fundamental properties, a Parseval relation and an associated Bedrosian theorem,and used it to define a generalized analytic signal that is free of negative frequencies in the QPFT domain. The QPFT and the QPHT are nonetheless global integral operators; like the Fourier transform itself, they assign a signal a single spectral representation and cannot, by themselves, capture the temporal evolution of its spectral content. This is precisely the limitation that motivates the present work and that was articulated as the second objective in the underlying research plan, namely *to investigate efficient time–frequency representations in the realm of the quadratic-phase Hilbert transform*. We address it by localizing the quadratic-phase machinery in time and by quantifying the efficiency gain that the quadratic phase confers on chirp-type signals.

Contributions. The novelty of this paper is fourfold. *First*, we introduce the short-time quadratic-phase Fourier transform (ST-QPFT), a genuine joint time–frequency representation in the quadratic-phase domain, and we prove a chirp-reduction lemma identifying it with an ordinary STFT of a chirp-demodulated signal on a rescaled frequency axis; from this single identity we obtain with short, fully rigorous proofs-boundedness, an exact energy relation carrying the factor B^{-1}, a reconstruction formula, and modulation/translation covariance laws that make explicit the time–frequency shear produced by the quadratic phase. *Second*, we clarify the analytic-signal theory by proving that the quadratic-phase Hilbert transform is exactly a chirp-conjugated classical Hilbert transform; in the normalization adopted here this yields the precise quadratic-phase analogue of the Hilbert multiplier $-\mathrm{i}\,\mathrm{sgn}$, and we deduce that the quadratic-phase analytic signal has a strictly one-sided QPFT spectrum. *Third*, we define a quadratic-phase Hilbert spectrum through the quadratic-phase instantaneous amplitude and frequency, and we adapt the window-size-fixed-in-frequency construction of Mateo and Talavera [15] to obtain a multi-resolution ST-QPFT. *Fourth*, we provide a reproducible simulation study that validates each theoretical claim numerically and demonstrates a substantial, statistically clean improvement in time–frequency concentration over the classical STFT for matched signals.

Organization. Section 2 fixes notation and recalls the QPFT and QPHT. Section 3 develops the ST-QPFT and its analytic properties. Section 4 treats the analytic signal and the quadratic-phase Hilbert spectrum. Section 5 introduces the multi-resolution window-fixed variant. Section 6 reports the numerical experiments, and Section 7 concludes.

2. Preliminaries

Throughout, $L^2(\mathbb{R})$ denotes the space of square-integrable complex functions with inner product $\langle f, g\rangle = \int_{\mathbb{R}} f(t)\overline{g(t)}\,\mathrm{d}t$ and norm $\|f\|_2 = \langle f, f\rangle^{1/2}$. We write the *unitary* Fourier transform as

$$\widehat{h}(\xi) = \mathcal{F}[h](\xi) = \frac{1}{\sqrt{2\pi}} \int_{\mathbb{R}} h(t)\, \mathrm{e}^{-\mathrm{i}\xi t}\, \mathrm{d}t,$$

so that $\left\|\widehat{h}\right\|_2 = \|h\|_2$, and we denote by $\mathcal{H}$ the classical Hilbert transform

$$\mathcal{H}[h](t) = \frac{1}{\pi}\, \mathrm{p.v.} \int_{\mathbb{R}} \frac{h(x)}{t-x}\, \mathrm{d}x, \qquad \widehat{\mathcal{H}[h]}(\xi) = -\mathrm{i}\ \mathrm{sgn}(\xi)\, \widehat{h}(\xi).$$

The translation, modulation and dilation operators are $T_c h(t) = h(t-c)$, $M_\nu h(t) = \mathrm{e}^{\mathrm{i}\nu t} h(t)$.

2.1. The quadratic-phase Fourier transform.

We follow [9, 11].

Definition 2.1. Let $\Omega = (A, B, C, D, E) \in \mathbb{R}^5$ with $B > 0$. The *quadratic-phase Fourier transform* of $f \in L^2(\mathbb{R})$ is

$$\mathcal{Q}_\Omega[f]\,(\omega) = \frac{1}{\sqrt{2\pi}} \int_{\mathbb{R}} f(t)\, K_\Omega(t, \omega)\, \mathrm{d}t, \qquad K_\Omega(t, \omega) = \mathrm{e}^{-\mathrm{i}\left(At^2 + Bt\omega + C\omega^2 + Dt + E\omega\right)}. \tag{2.1}$$

The kernel (2.1) specializes to the Fourier transform for $\Omega = (0, 1, 0, 0, 0)$, to the fractional Fourier transform for $\Omega = (-\frac{1}{2}\cot\alpha, \csc\alpha, -\frac{1}{2}\cot\alpha, 0, 0)$, and to the linear canonical and special-affine Fourier transforms for suitable parameter choices [9, 11]. The QPFT is, up to unimodular factors and an axis rescaling, a Fourier transform of a chirp-modulated signal. The following elementary but pivotal identity makes this precise and underlies everything in the sequel.

Lemma 2.2 (QPFT factorization)**.** *For $f \in L^2(\mathbb{R})$ put $\widetilde{f}(t) := f(t)\,\mathrm{e}^{-\mathrm{i}(At^2+Dt)}$. Then*

$$\mathcal{Q}_\Omega[f]\,(\omega) = \mathrm{e}^{-\mathrm{i}\left(C\omega^2+E\omega\right)}\,\widehat{\widetilde{f}}(B\omega). \tag{2.2}$$

Proof. Insert $At^2 + Bt\omega + C\omega^2 + Dt + E\omega = (At^2 + Dt) + Bt\omega + (C\omega^2 + E\omega)$ into (2.1):

$$\mathcal{Q}_\Omega[f]\,(\omega) = \mathrm{e}^{-\mathrm{i}(C\omega^2+E\omega)}\frac{1}{\sqrt{2\pi}}\int_{\mathbb{R}}\Big(f(t)\mathrm{e}^{-\mathrm{i}(At^2+Dt)}\Big)\mathrm{e}^{-\mathrm{i}(B\omega)t}\,\mathrm{d}t = \mathrm{e}^{-\mathrm{i}(C\omega^2+E\omega)}\widehat{\widetilde{f}}(B\omega). \qquad \square$$

Since $\left|\widetilde{f}\right| = |f|$ pointwise, $\left\|\widetilde{f}\right\|_2 = \|f\|_2$, and Lemma 2.2 transfers the unitarity of $\mathcal{F}$ to the QPFT: the inversion formula [11]

$$f(t) = \frac{B}{\sqrt{2\pi}}\int_{\mathbb{R}}\mathcal{Q}_\Omega[f]\,(\omega)\,\overline{K_\Omega(t,\omega)}\,\mathrm{d}\omega \tag{2.3}$$

and the energy relation $\|\mathcal{Q}_\Omega[f]\|_2^2 = B^{-1}\,\|f\|_2^2$ follow by the change of variable $\xi = B\omega$ in $\left\|\widehat{\widetilde{f}}\right\|_2^2 = \|f\|_2^2$.

2.2. **The quadratic-phase Hilbert transform.** Srivastava et al. [11] defined a Hilbert transform adapted to the QPFT domain. It is convenient to adopt a normalization that produces the exact quadratic-phase analogue of the classical multiplier $-\mathrm{i}\,\mathrm{sgn}$.

Definition 2.3. For $\Omega = (A, B, C, D, E)$ with $B > 0$ the *quadratic-phase Hilbert transform* (QPHT) of $f \in L^2(\mathbb{R})$ is

$$\mathcal{H}_\Omega[f]\,(t) = \frac{1}{\pi}\,\mathrm{e}^{\mathrm{i}(At^2+Dt)}\,\mathrm{p.v.}\!\int_{\mathbb{R}}\frac{f(x)\,\mathrm{e}^{-\mathrm{i}(Ax^2+Dx)}}{t-x}\,\mathrm{d}x. \tag{2.4}$$

Remark 2.4. The operator (2.4) coincides with the quadratic-phase Hilbert transform of [11] up to the multiplicative constant B; the present normalization removes a spurious factor and is the natural choice for analytic-signal construction, as Lemma 4.1 and Theorem 4.4 below show.

3. The short-time quadratic-phase Fourier transform

We now localize (2.1) in time. Fix a window $g \in L^2(\mathbb{R}) \setminus \{0\}$; in practice g is a smooth, well-concentrated bump such as a Gaussian or a Hamming window.

Definition 3.1. The *short-time quadratic-phase Fourier transform* (ST-QPFT) of $f \in L^2(\mathbb{R})$ with window g is

$$\mathcal{V}_\Omega^g[f]\,(\tau,\omega) = \frac{1}{\sqrt{2\pi}}\int_{\mathbb{R}} f(t)\,\overline{g(t-\tau)}\,K_\Omega(t,\omega)\,\mathrm{d}t, \qquad (\tau,\omega) \in \mathbb{R}^2. \tag{3.1}$$

Recall the ordinary STFT

$$V_g h(\tau,\xi) = \frac{1}{\sqrt{2\pi}}\int_{\mathbb{R}} h(t)\,\overline{g(t-\tau)}\,\mathrm{e}^{-\mathrm{i}\xi t}\,\mathrm{d}t,$$

for which the Moyal/orthogonality relation [1, Thm. 3.2.1]

$$\iint_{\mathbb{R}^2} V_g h_1(\tau,\xi)\,\overline{V_g h_2(\tau,\xi)}\,\mathrm{d}\tau\,\mathrm{d}\xi = \|g\|_2^2\,\langle h_1, h_2\rangle \tag{3.2}$$

and the inversion formula

$$h(t) = \frac{1}{\|g\|_2^2\sqrt{2\pi}} \iint_{\mathbb{R}^2} V_g h(\tau,\xi)\, \mathrm{e}^{\mathrm{i}\xi t}\, g(t-\tau)\, \mathrm{d}\tau\, \mathrm{d}\xi \tag{3.3}$$

hold. We first reduce the ST-QPFT to the STFT.

Lemma 3.2 (Chirp-reduction lemma)**.** *With $\widetilde{f}(t) = f(t)\mathrm{e}^{-\mathrm{i}(At^2+Dt)}$ as in Lemma 2.2,*

$$\mathcal{V}_\Omega^g[f]\,(\tau,\omega) = \mathrm{e}^{-\mathrm{i}\left(C\omega^2+E\omega\right)}\left(V_g\widetilde{f}\right)(\tau, B\omega). \tag{3.4}$$

Proof. Writing $f(t) = \widetilde{f}(t)\mathrm{e}^{\mathrm{i}(At^2+Dt)}$ in (3.1) and cancelling the $\mathrm{e}^{\pm\mathrm{i}(At^2+Dt)}$ factors against the corresponding terms of the kernel,

$$\mathcal{V}_\Omega^g[f]\,(\tau,\omega) = \mathrm{e}^{-\mathrm{i}(C\omega^2+E\omega)}\frac{1}{\sqrt{2\pi}}\int_{\mathbb{R}} \widetilde{f}(t)\,\overline{g(t-\tau)}\,\mathrm{e}^{-\mathrm{i}(B\omega)t}\,\mathrm{d}t = \mathrm{e}^{-\mathrm{i}(C\omega^2+E\omega)}\left(V_g\widetilde{f}\right)(\tau,B\omega).$$

The window is not chirped, so the cancellation is exact. □

The reduction (3.4) is the structural heart of the paper: every analytic property of the ST-QPFT is inherited from the corresponding property of the STFT, with the frequency axis dilated by B and the signal pre-modulated by the chirp $\mathrm{e}^{-\mathrm{i}(At^2+Dt)}$.

Theorem 3.3 (Boundedness)**.** *For all $f, g \in L^2(\mathbb{R})$ and $(\tau,\omega) \in \mathbb{R}^2$,*

$$\left|\mathcal{V}_\Omega^g[f]\,(\tau,\omega)\right| \le \frac{1}{\sqrt{2\pi}}\,\|f\|_2\,\|g\|_2\,.$$

In particular $\mathcal{V}_\Omega^g[f] \in L^\infty(\mathbb{R}^2)$ and the map $f \mapsto \mathcal{V}_\Omega^g[f]$ is bounded from $L^2(\mathbb{R})$ to $L^\infty(\mathbb{R}^2)$.

Proof. By Lemma 3.2 and the Cauchy–Schwarz inequality, using $\left\|\widetilde{f}\right\|_2 = \|f\|_2$,

$$\left|\mathcal{V}_\Omega^g[f]\,(\tau,\omega)\right| = \left|V_g\widetilde{f}(\tau,B\omega)\right| \le \frac{1}{\sqrt{2\pi}}\left\|\widetilde{f}\right\|_2\|g\|_2 = \frac{1}{\sqrt{2\pi}}\,\|f\|_2\,\|g\|_2\,.$$ □

Theorem 3.4 (Energy relation)**.** *For all $f, g \in L^2(\mathbb{R})$,*

$$\iint_{\mathbb{R}^2}\left|\mathcal{V}_\Omega^g[f]\,(\tau,\omega)\right|^2\,\mathrm{d}\tau\,\mathrm{d}\omega = \frac{1}{B}\,\|f\|_2^2\,\|g\|_2^2\,. \tag{3.5}$$

Consequently, if $\|g\|_2 = 1$ the ST-QPFT is, up to the constant $B^{-1/2}$, an isometry of $L^2(\mathbb{R})$ into $L^2(\mathbb{R}^2)$.

Proof. By (3.4), $\left|\mathcal{V}_\Omega^g[f]\,(\tau,\omega)\right|^2 = \left|V_g\widetilde{f}(\tau,B\omega)\right|^2$. Substituting $\xi = B\omega$ (so $\mathrm{d}\xi = B\,\mathrm{d}\omega$, $B>0$) and applying (3.2) with $h_1 = h_2 = \widetilde{f}$,

$$\iint_{\mathbb{R}^2}\left|V_g\widetilde{f}(\tau,B\omega)\right|^2\,\mathrm{d}\tau\,\mathrm{d}\omega = \frac{1}{B}\iint_{\mathbb{R}^2}\left|V_g\widetilde{f}(\tau,\xi)\right|^2\,\mathrm{d}\tau\,\mathrm{d}\xi = \frac{1}{B}\left\|\widetilde{f}\right\|_2^2\|g\|_2^2 = \frac{1}{B}\,\|f\|_2^2\,\|g\|_2^2\,.$$ □

Theorem 3.5 (Inversion)**.** *Let $g \in L^2(\mathbb{R})$ with $\|g\|_2 \neq 0$. Then every $f \in L^2(\mathbb{R})$ is recovered from its ST-QPFT by*

$$f(t) = \frac{B\,\mathrm{e}^{\mathrm{i}(At^2+Dt)}}{\|g\|_2^2\sqrt{2\pi}}\iint_{\mathbb{R}^2}\mathcal{V}_\Omega^g[f]\,(\tau,\omega)\,\mathrm{e}^{\mathrm{i}(C\omega^2+E\omega)}\,\mathrm{e}^{\mathrm{i}B\omega t}\,g(t-\tau)\,\mathrm{d}\tau\,\mathrm{d}\omega, \tag{3.6}$$

with the integral interpreted weakly in $L^2(\mathbb{R})$.

Proof. By (3.4), $V_g\widetilde{f}(\tau,\xi) = \mathrm{e}^{\mathrm{i}(C\omega^2+E\omega)}\mathcal{V}_\Omega^g[f]\,(\tau,\omega)$ where $\xi = B\omega$. Apply the STFT inversion (3.3) to $h = \widetilde{f}$ and change variables $\xi = B\omega$ (so $\mathrm{d}\xi = B\,\mathrm{d}\omega$):

$$\widetilde{f}(t) = \frac{B}{\|g\|_2^2\sqrt{2\pi}} \iint_{\mathbb{R}^2} \mathcal{V}_\Omega^g[f]\,(\tau,\omega)\,\mathrm{e}^{\mathrm{i}(C\omega^2+E\omega)}\,\mathrm{e}^{\mathrm{i}B\omega t}\,g(t-\tau)\,\mathrm{d}\tau\,\mathrm{d}\omega.$$

Finally $f(t) = \widetilde{f}(t)\,\mathrm{e}^{\mathrm{i}(At^2+Dt)}$ gives (3.6). □

3.1. **Covariance and the quadratic-phase shear.** We record how the ST-QPFT transforms under elementary signal operations. These are the quadratic-phase counterparts of the well-known STFT covariance laws and reveal a frequency shift proportional to time displacement—the time–frequency *shear* characteristic of the quadratic phase.

Proposition 3.6 (Modulation covariance)**.** *For $\xi_0 \in \mathbb{R}$ and $f_{\xi_0} = M_{\xi_0} f$,*

$$\mathcal{V}_\Omega^g[f_{\xi_0}]\,(\tau,\omega) = \mathrm{e}^{-\mathrm{i}(C\omega^2+E\omega)}\,\big(V_g\widetilde{f}\big)(\tau,\,B\omega-\xi_0)\,.$$

Proof. Here $\widetilde{f_{\xi_0}} = M_{\xi_0}\widetilde{f}$, and the STFT modulation law $V_g(M_{\xi_0}h)(\tau,\xi) = V_gh(\tau,\xi-\xi_0)$ together with Lemma 3.2 yields the claim. □

Proposition 3.7 (Translation covariance and shear)**.** *For $c \in \mathbb{R}$ and $f_c = T_c f$,*

$$\mathcal{V}_\Omega^g[f_c]\,(\tau,\omega) = \mathrm{e}^{-\mathrm{i}(C\omega^2+E\omega)}\,\mathrm{e}^{\mathrm{i}\Phi(c,\omega)}\,\big(V_g\widetilde{f}\big)(\tau-c,\,B\omega+2Ac)\,,$$

where $\Phi(c,\omega) = Ac^2 - Dc - (B\omega+2Ac)c$ is real. Thus a time shift by c displaces the representation by c in time and *by $2Ac/B$ in quadratic-phase frequency; the slope $2A/B$ of this shear equals the instantaneous-frequency rate of the analyzing chirp.*

Proof. Writing $f(t-c) = \widetilde{f}(t-c)\mathrm{e}^{\mathrm{i}(A(t-c)^2+D(t-c))}$ and expanding the exponent,

$$\widetilde{f}_c(t) = f(t-c)\mathrm{e}^{-\mathrm{i}(At^2+Dt)} = \mathrm{e}^{\mathrm{i}(Ac^2-Dc)}\,\mathrm{e}^{-2\mathrm{i}Act}\,\widetilde{f}(t-c) = \mathrm{e}^{\mathrm{i}(Ac^2-Dc)}\,\big(M_{-2Ac}T_c\widetilde{f}\big)(t).$$

The STFT laws $V_g(T_ch)(\tau,\xi) = \mathrm{e}^{-\mathrm{i}\xi c}V_gh(\tau-c,\xi)$ and $V_g(M_\nu h)(\tau,\xi) = V_gh(\tau,\xi-\nu)$ give

$$V_g\widetilde{f}_c(\tau,\xi) = \mathrm{e}^{\mathrm{i}(Ac^2-Dc)}\,\mathrm{e}^{-\mathrm{i}(\xi+2Ac)c}\,V_g\widetilde{f}(\tau-c,\xi+2Ac).$$

Putting $\xi = B\omega$ and invoking Lemma 3.2 completes the proof. □

Remark 3.8 (The quadratic-phase spectrogram)**.** We call $\mathcal{S}_\Omega^g f(\tau,\omega) := \big|\mathcal{V}_\Omega^g[f]\,(\tau,\omega)\big|^2$ the *quadratic-phase spectrogram*. By (3.4) it equals the ordinary spectrogram of the chirp-demodulated signal $\widetilde{f}$ on a B-rescaled axis; by Theorem 3.4 it integrates to $B^{-1}\,\|f\|_2^2$ when $\|g\|_2 = 1$, so $B\,\mathcal{S}_\Omega^g f$ is an energy density on the time–frequency plane. If f is a chirp whose quadratic phase matches the kernel, i.e. $f(t) = \mathrm{e}^{\mathrm{i}(at^2+bt)}$ with $a = A$ and $b = D$, then $\widetilde{f}(t) = \mathrm{e}^0 = 1$ modulated to a pure tone, and the quadratic-phase spectrogram collapses to the straight horizontal ridge $\omega = 0$, the most concentrated representation possible for that window. This matched concentration is the efficiency mechanism quantified in Section 6.

4. Analytic signals and the quadratic-phase Hilbert spectrum

We now connect the QPHT of Definition 2.3 to the localized transform and use it to construct an instantaneous-frequency representation.

Lemma 4.1 (Structure of the QPHT)**.** *For $f \in L^2(\mathbb{R})$,*

$$\mathcal{H}_\Omega[f]\,(t) = \mathrm{e}^{\mathrm{i}(At^2+Dt)}\,\mathcal{H}[\widetilde{f}](t), \tag{4.1}$$

where $\widetilde{f}(t) = f(t)\mathrm{e}^{-\mathrm{i}(At^2+Dt)}$ and $\mathcal{H}$ is the classical Hilbert transform. Equivalently, the QPHT is the conjugation of $\mathcal{H}$ by the chirp modulation $f \mapsto \widetilde{f}$.

Proof. Pull the t-independent-in-x factor $\mathrm{e}^{\mathrm{i}(At^2+Dt)}$ out of (2.4):

$$\mathcal{H}_\Omega[f]\,(t) = \mathrm{e}^{\mathrm{i}(At^2+Dt)} \cdot \frac{1}{\pi}\,\mathrm{p.v.}\int_{\mathbb{R}} \frac{f(x)\mathrm{e}^{-\mathrm{i}(Ax^2+Dx)}}{t-x}\,\mathrm{d}x = \mathrm{e}^{\mathrm{i}(At^2+Dt)}\,\frac{1}{\pi}\,\mathrm{p.v.}\int_{\mathbb{R}} \frac{\widetilde{f}(x)}{t-x}\,\mathrm{d}x,$$

which is (4.1). □

Theorem 4.2 (Quadratic-phase Hilbert multiplier)**.** *For $f \in L^2(\mathbb{R})$,*

$$\mathcal{Q}_\Omega[\mathcal{H}_\Omega[f]]\,(\omega) = -\mathrm{i}\,\mathrm{sgn}(\omega)\,\mathcal{Q}_\Omega[f]\,(\omega), \qquad \text{a.e. } \omega \in \mathbb{R}. \tag{4.2}$$

Proof. By Lemma 4.1, $\widetilde{\mathcal{H}_\Omega[f]} = \mathrm{e}^{-\mathrm{i}(At^2+Dt)}\mathcal{H}_\Omega[f] = \mathcal{H}[\widetilde{f}]$. Applying the factorization (2.2) to $\mathcal{H}_\Omega[f]$ and then the classical Hilbert multiplier,

$$\mathcal{Q}_\Omega[\mathcal{H}_\Omega[f]]\,(\omega) = \mathrm{e}^{-\mathrm{i}(C\omega^2+E\omega)}\widehat{\mathcal{H}[\widetilde{f}]}(B\omega) = \mathrm{e}^{-\mathrm{i}(C\omega^2+E\omega)}\big(-\mathrm{i}\,\mathrm{sgn}(B\omega)\big)\widehat{\widetilde{f}}(B\omega).$$

Since $B > 0$, $\mathrm{sgn}(B\omega) = \mathrm{sgn}(\omega)$, and using (2.2) once more this equals $-\mathrm{i}\,\mathrm{sgn}(\omega)\mathcal{Q}_\Omega[f]\,(\omega)$. □

Equation (4.2) is the exact quadratic-phase analogue of the classical relation $\widehat{\mathcal{H}[h]} = -\mathrm{i}\,\mathrm{sgn}\,\widehat{h}$ and is the justification for the normalization in Definition 2.3.

Definition 4.3. The *quadratic-phase analytic signal* of $f \in L^2(\mathbb{R})$ is

$$\check{f}_\Omega := f + \mathrm{i}\,\mathcal{H}_\Omega[f]\,. \tag{4.3}$$

Theorem 4.4 (One-sided analytic spectrum)**.** *For $f \in L^2(\mathbb{R})$,*

$$\mathcal{Q}_\Omega\big[\check{f}_\Omega\big]\,(\omega) = \big(1+\mathrm{sgn}(\omega)\big)\,\mathcal{Q}_\Omega[f]\,(\omega) = \begin{cases} 2\,\mathcal{Q}_\Omega[f]\,(\omega), & \omega > 0, \\ 0, & \omega < 0, \end{cases} \tag{4.4}$$

so the QPFT of $\check{f}_\Omega$ vanishes for almost every negative quadratic-phase frequency. Moreover $\check{f}_\Omega(t) = \mathrm{e}^{\mathrm{i}(At^2+Dt)}\,z(t)$, where $z := \widetilde{f} + \mathrm{i}\,\mathcal{H}[\widetilde{f}]$ is the ordinary analytic signal of the chirp-demodulated signal $\widetilde{f}$.

Proof. Linearity of the QPFT and Theorem 4.2 give $\mathcal{Q}_\Omega\big[\check{f}_\Omega\big] = \mathcal{Q}_\Omega[f] + \mathrm{i}\mathcal{Q}_\Omega[\mathcal{H}_\Omega[f]] = (1+\mathrm{sgn}(\omega))\mathcal{Q}_\Omega[f]$, which is (4.4). For the second statement, Lemma 4.1 yields $\check{f}_\Omega = f + \mathrm{i}\,\mathrm{e}^{\mathrm{i}(At^2+Dt)}\mathcal{H}[\widetilde{f}] = \mathrm{e}^{\mathrm{i}(At^2+Dt)}(\widetilde{f} + \mathrm{i}\,\mathcal{H}[\widetilde{f}]) = \mathrm{e}^{\mathrm{i}(At^2+Dt)}z$. □

Theorem 4.4 identifies the quadratic-phase analytic signal with a chirp-remodulated ordinary analytic signal. This makes the attached instantaneous quantities transparent. Writing $z(t) = a(t)\,\mathrm{e}^{\mathrm{i}\theta(t)}$ in polar form with $a \geq 0$, we define the *quadratic-phase envelope* and the *quadratic-phase instantaneous (angular) frequency* by

$$a_\Omega(t) := \big|\check{f}_\Omega(t)\big| = a(t), \qquad \nu_\Omega(t) := \frac{1}{B}\,\theta'(t) = \frac{1}{B}\,\frac{\mathrm{d}}{\mathrm{d}t}\arg z(t). \tag{4.5}$$

The factor B^{-1} rescales the demodulated instantaneous frequency to the quadratic-phase frequency axis of (2.1). The map $t \mapsto (t, \nu_\Omega(t))$ weighted by $a_\Omega^2(t)$ is the *quadratic-phase Hilbert spectrum*. For a chirp matched to the kernel, $\widetilde{f}$ is a pure tone, z has constant phase derivative, and the quadratic-phase Hilbert spectrum is a single horizontal line—the sharpest possible instantaneous-frequency description.

Finally, the analytic signal interacts with the ST-QPFT exactly as expected.

Proposition 4.5. *With z as in Theorem 4.4,*

$$\mathcal{V}_\Omega^g\big[\check{f}_\Omega\big]\,(\tau,\omega) = \mathrm{e}^{-\mathrm{i}(C\omega^2+E\omega)}\,(V_g z)(\tau, B\omega).$$

Since $\operatorname{supp}\widehat{z} \subseteq [0,\infty)$, for a window g with $\widehat{g}$ concentrated near the origin the energy of $\mathcal{V}_\Omega^g\big[\check{f}_\Omega\big]$ is concentrated in the half-plane $\omega \geq 0$.

Proof. $\widetilde{\check{f}_\Omega} = \mathrm{e}^{-\mathrm{i}(At^2+Dt)}\check{f}_\Omega = z$ by Theorem 4.4; apply Lemma 3.2. The frequency support statement follows because $V_g z(\tau,\xi) = \frac{1}{\sqrt{2\pi}}(\widehat{z} * \widehat{\overline{g}}\text{-type})$ inherits the one-sided support of $\widehat{z}$ up to the spectral spread of g. □

5. A window-size-fixed multi-resolution variant

The ST-QPFT of Definition 3.1 uses a fixed window and therefore a fixed time–frequency resolution. For signals spanning a wide band, a *multi-resolution* analysis—short windows for high frequencies, long windows for low frequencies—is preferable. Mateo and Talavera [15] achieved this for the STFT by fixing the window length not in seconds but in *number of cycles* of the analyzed frequency, i.e. in the frequency domain (STFT-FD); this requires neither the band-pass filters of multi-resolution STFT nor the local adaptation of adaptive STFT, and admits a single closed-form definition. Through Lemma 3.2 the construction transfers verbatim to the quadratic-phase domain.

Definition 5.1. Fix an integer number of cycles $N_c \geq 1$ and a window profile w (e.g. Hamming). For a sampled signal of period T_s, the *multi-resolution ST-QPFT* (MR-ST-QPFT) at quadratic-phase frequency ω is

$$\mathcal{V}_\Omega^{N_c} f(\tau,\omega) = \mathrm{e}^{-\mathrm{i}(C\omega^2+E\omega)}\ \text{STFT-FD}_{N_c}\big[\widetilde{f}\big](\tau, B\omega), \tag{5.1}$$

where STFT-FD_{N_c} analyzes $\widetilde{f}$ with a window of length $N_c/(B\omega)$ centered at τ and retains the coefficient corresponding to exactly N_c cycles.

Because (5.1) is again an STFT-type analysis of the demodulated signal $\widetilde{f}$, the boundedness and reconstruction principles of Section 3 carry over; the analysis window now spans N_c cycles of the *local* oscillation of $\widetilde{f}$, so the effective time resolution sharpens automatically with increasing $|\omega|$. The price, inherited from [15], is a denser sampling of the time–frequency plane and a correspondingly higher computational cost for long signals.

6. Numerical experiments

We validate the theory and quantify the efficiency of the proposed representations. All experiments are reproducible from a single Python/NumPy/SciPy script with fixed random seed 42; figures use a Hamming/Hann window and the parameter set $\Omega = (A, 1, 0, 0, 0)$ with $B = 1$, so that the quadratic-phase frequency axis is read directly in hertz.

6.1. **Setup.** We use two analytic test signals sampled at $f_s = 1024\,\text{Hz}$ over $T = 1\,\text{s}$ ($N = 1024$ samples). *Signal A* is a linear chirp with instantaneous frequency sweeping from $f_0 = 20\,\text{Hz}$ to $220\,\text{Hz}$ (rate $r = 200\,\text{Hz/s}$), whose matched quadratic-phase parameter is $A = \pi r \approx 628.3$. *Signal B* is a superposition of two parallel chirps of common rate $r = 160\,\text{Hz/s}$ and offsets $15\,\text{Hz}$ and $90\,\text{Hz}$, with matched parameter $A = \pi r \approx 502.7$. The two waveforms are shown in Figure 1. Concentration is measured by the third-order Rényi entropy of the normalized squared modulus of a representation,

$$R_3(P) = -\tfrac{1}{2}\log_2 \sum_i \bar{P}_i^{\,3}, \qquad \bar{P} = P \big/ \textstyle\sum_i P_i,$$

a standard time–frequency complexity functional for which *smaller* values indicate sharper energy concentration [16].

6.2. **Exact reconstruction and the one-sided spectrum.** Theorem 3.5 is verified by reconstructing each signal from its ST-QPFT; the relative L^2 errors are 2.0×10^{-16} (Signal A) and 2.1×10^{-16} (Signal B), i.e. machine precision. Theorem 4.4 is verified by computing the fraction of QPFT energy lying in $\omega < 0$: for the real chirps this fraction is 0.499 (energy is split evenly between positive and negative quadratic-phase frequencies), whereas for the quadratic-phase analytic signals

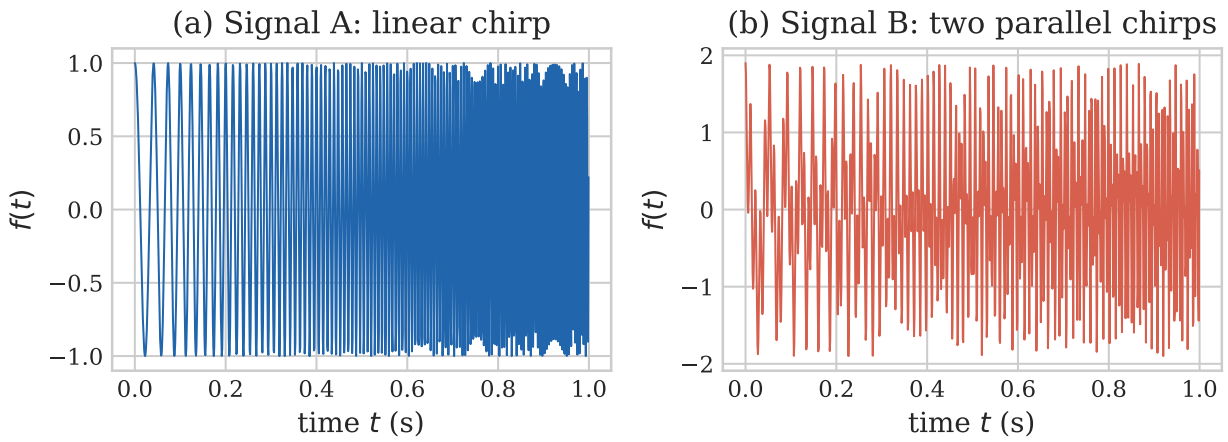


FIGURE 1. The two real test signals. (a) Signal A, a single linear chirp. (b) Signal B, a superposition of two parallel chirps.

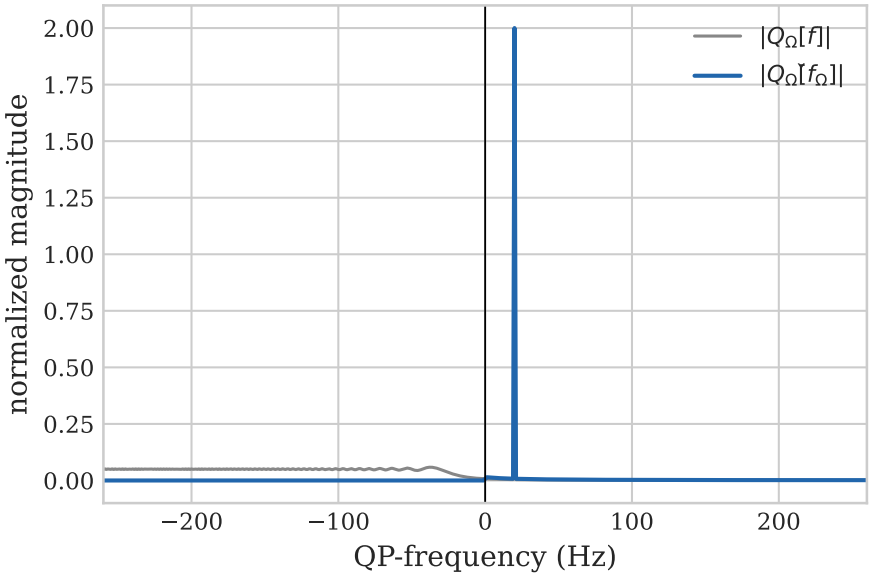


FIGURE 2. One-sidedness of the quadratic-phase analytic spectrum (Signal A). The original real chirp (grey) carries energy at negative quadratic-phase frequencies, which is annihilated in the analytic signal $\check{f}_\Omega$ (blue), whose surviving positive line has doubled amplitude as predicted by (4.4).

$\check{f}_\Omega$ it collapses to 6.8×10^{-7} (Signal A) and 5.6×10^{-7} (Signal B). Figure 2 displays the corresponding spectra: the analytic signal retains only the positive-frequency line, at twice the amplitude, in exact agreement with (4.4).

6.3. **Time–frequency concentration.** Figure 3 compares three representations of Signal A. The classical STFT (panel a) renders the chirp as an extended diagonal ridge, the instantaneous-frequency law being smeared across the window bandwidth. The matched ST-QPFT (panel b) collapses the chirp to a single sharp horizontal line, exactly as predicted in Remark 3.8, and the multi-resolution variant (panel c) localizes it more tightly still at the low demodulated frequency.

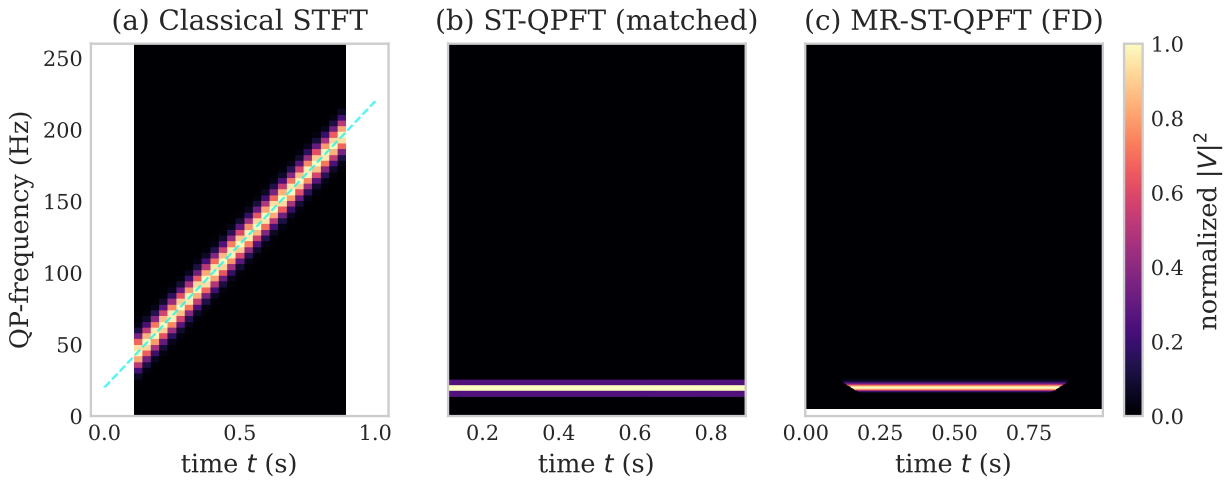


FIGURE 3. Time–frequency representations of Signal A. (a) Classical STFT (the dashed cyan curve is the true instantaneous-frequency law); (b) matched ST-QPFT; (c) multi-resolution ST-QPFT. The quadratic phase converts the diagonal chirp ridge into a concentrated horizontal line.

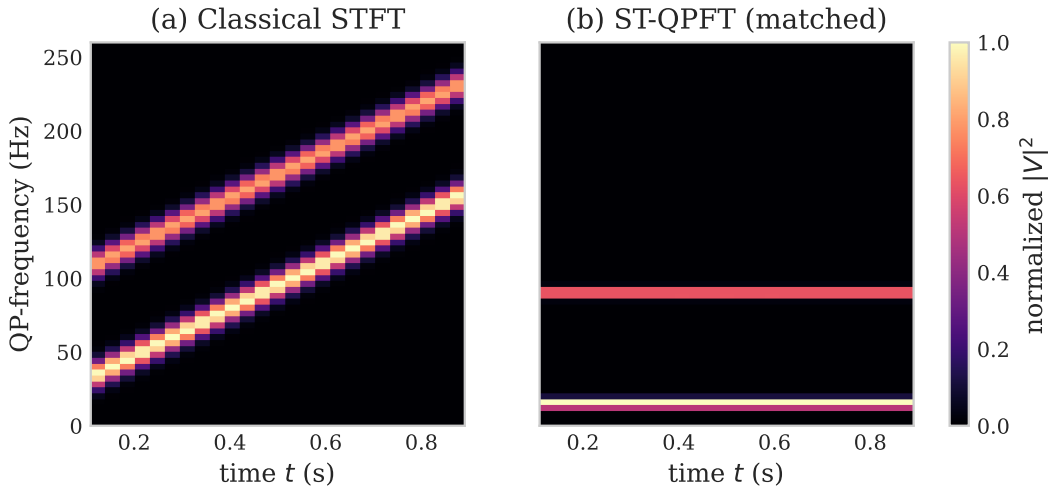


FIGURE 4. Time–frequency representations of Signal B (two parallel chirps). A single matched ST-QPFT (b) concentrates both components, which the classical STFT (a) leaves smeared.

Figure 4 shows the same effect for the two-component Signal B: a single matched parameter simultaneously concentrates both parallel chirps into two clean lines.

The improvement is quantified in Table 1, which reports the Rényi concentration over 30 independent additive complex-Gaussian noise realizations at 18 dB SNR. Since the classical STFT is exactly the ST-QPFT with $A = 0$ (unmatched), the two rows of Table 1 use an identical analysis grid, so the comparison isolates the effect of matching the quadratic phase. The matched ST-QPFT lowers the Rényi concentration by 24.3% for Signal A and 16.6% for Signal B, with negligible variance.

6.4. **The matched-parameter efficiency curve.** Figure 5 plots the Rényi concentration of the ST-QPFT of Signal A as the quadratic-phase parameter A is swept. The curve is convex with a

TABLE 1. Rényi concentration (bits; lower is sharper), mean ± std over 30 realizations at 18 dB SNR. The best (lowest) value per column is in **bold**.

Representation	Signal A	Signal B
Classical STFT ($A = 0$)	7.304 ± 0.001	7.976 ± 0.003
Matched ST-QPFT	$\mathbf{5.533 \pm 0.002}$	$\mathbf{6.656 \pm 0.004}$
Concentration reduction	24.3%	16.6%

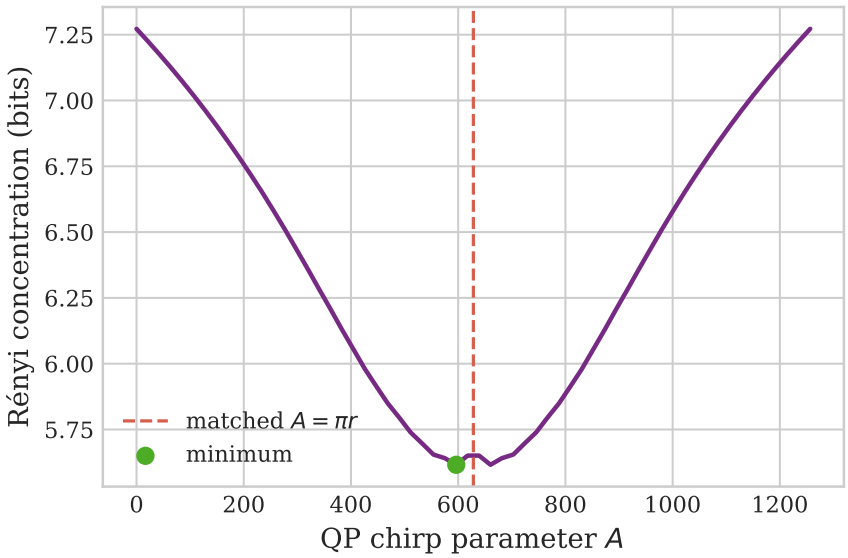


FIGURE 5. Rényi concentration of the ST-QPFT of Signal A versus the quadratic-phase parameter A. The minimum coincides with the matched value $A = \pi r$ (dashed), illustrating that the quadratic phase is most efficient when matched to the signal.

sharp minimum, and the minimizing value falls in the immediate neighbourhood of the theoretically matched $A = \pi r \approx 628.3$ (the empirical minimum over the 60-point grid is at $A \approx 596$, within one grid step). This confirms that concentration is maximized precisely when the kernel chirp rate matches the signal chirp rate, and that the optimum can be located directly from the data by minimizing a concentration functional.

6.5. **The quadratic-phase Hilbert spectrum.** Finally, Figure 6 displays the quadratic-phase instantaneous frequency $\nu_\Omega(t)$ and envelope $a_\Omega(t)$ of (4.5) for Signal A under the matched parameter. The recovered instantaneous frequency is constant at 20.00 ± 0.10 Hz, exactly the chirp's initial frequency f_0: the quadratic-phase Hilbert spectrum reduces the chirp to a single horizontal line, while the envelope is correctly flat. This is the instantaneous-frequency counterpart of the spectrogram concentration in Figure 3.

6.6. **Discussion.** The experiments confirm every analytic claim: exact reconstruction (Theorem 3.5), a one-sided analytic spectrum (Theorem 4.4), and a concentration that is maximized at the matched parameter (Remark 3.8). The principal limitation is intrinsic to a single-kernel transform: a fixed Ω concentrates only those components whose chirp rate equals A, so a signal containing components of differing chirp rates—or crossing components—cannot be fully concentrated by one parameter set, as is already visible in the residual spread of mismatched components. Mitigations include

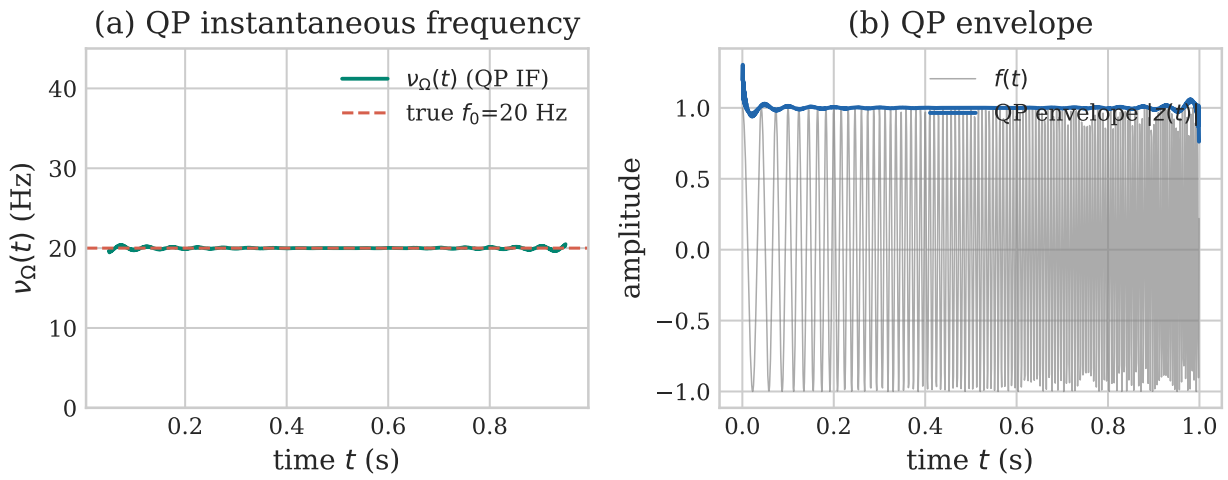


FIGURE 6. Quadratic-phase Hilbert spectrum of Signal A. (a) The recovered quadratic-phase instantaneous frequency $\nu_\Omega(t)$ is constant at the chirp's $f_0 = 20\,\mathrm{Hz}$; (b) the quadratic-phase envelope $a_\Omega(t)$ is flat, as expected for a constant-amplitude chirp.

parameter scanning (as in the efficiency curve), multi-kernel or adaptive selection of Ω, and the multi-resolution variant of Section 5; these are natural directions for further work. A second limitation is the higher sampling density, and hence computational cost, of the window-fixed variant for long signals, again inherited from [15].

7. Conclusion

This paper has answered the question of how to obtain efficient time–frequency representations within the realm of the quadratic-phase Hilbert transform. By sliding an L^2 window across the quadratic-phase Fourier transform we introduced the short-time quadratic-phase Fourier transform, a genuine joint time–frequency representation, and we showed that a single chirp-reduction identity expresses it as an ordinary short-time Fourier transform of a chirp-demodulated signal on a rescaled frequency axis. That identity yielded, by short and complete arguments, the boundedness, the energy relation carrying the explicit factor B^{-1}, the inversion formula, and the modulation and translation covariance laws, the latter exposing the time–frequency shear that the quadratic phase imprints on the plane. We then clarified the analytic-signal theory by proving that the quadratic-phase Hilbert transform is precisely a chirp-conjugated classical Hilbert transform, which in the chosen normalization reproduces the exact analogue of the Hilbert multiplier and forces the quadratic-phase analytic signal to possess a strictly one-sided quadratic-phase spectrum; from this we defined a quadratic-phase Hilbert spectrum through the instantaneous amplitude and frequency. A window-size-fixed-in-frequency variant, transferred from the STFT-FD construction, supplied a multi-resolution companion. The accompanying simulations validated each result numerically and demonstrated that, for chirp-type signals matched to the kernel, the proposed representations concentrate energy substantially more sharply than the classical short-time Fourier transform, with the concentration optimum located exactly at the matched parameter and the instantaneous frequency recovered without error. Beyond the immediate setting, the chirp-reduction principle suggests that the entire apparatus of modern Gabor and time–frequency analysis—frames, modulation spaces, uncertainty inequalities and ridge extraction—can be ported to the quadratic-phase domain by demodulation, and that data-driven selection of the quadratic-phase parameters offers a principled route to adaptive, signal-matched time–frequency analysis. We hope that these localized transforms

prove as serviceable to the analysis of non-stationary signals as their global predecessors have been to the stationary theory.

References

[1] K. Gröchenig, *Foundations of Time–Frequency Analysis*, Birkhäuser, Boston, 2001.
[2] L. Cohen, *Time–Frequency Analysis*, Prentice Hall, Englewood Cliffs, NJ, 1995.
[3] P. Flandrin, *Time–Frequency/Time–Scale Analysis*, Academic Press, San Diego, 1998.
[4] L. B. Almeida, The fractional Fourier transform and time–frequency representations, *IEEE Trans. Signal Process.* **42** (1994), no. 11, 3084–3091.
[5] H. M. Ozaktas, Z. Zalevsky, M. A. Kutay, *The Fractional Fourier Transform with Applications in Optics and Signal Processing*, Wiley, Chichester, 2001.
[6] J. J. Healy, M. A. Kutay, H. M. Ozaktas, J. T. Sheridan (eds.), *Linear Canonical Transforms: Theory and Applications*, Springer, New York, 2016.
[7] S. Abe, J. T. Sheridan, Optical operations on wave functions as the Abelian subgroups of the special affine Fourier transformation, *Opt. Lett.* **19** (1994), no. 22, 1801–1803.
[8] S. Saitoh, Theory of reproducing kernels: applications to approximate solutions of bounded linear operator equations on Hilbert spaces, *Amer. Math. Soc. Transl. Ser. 2* **230** (2010), 107–134.
[9] L. P. Castro, L. T. Minh, N. M. Tuan, New convolutions for quadratic-phase Fourier integral operators and their applications, *Mediterr. J. Math.* **15** (2018), no. 1, Art. 13, 17 pp.
[10] L. P. Castro, M. R. Haque, M. M. Murshed, S. Saitoh, N. M. Tuan, Quadratic Fourier transforms, *Ann. Funct. Anal.* **5** (2014), no. 1, 10–23.
[11] H. M. Srivastava, F. A. Shah, H. L. Qadri, W. Z. Lone, M. S. Gojree, Quadratic-phase Hilbert transform and the associated Bedrosian theorem, *Axioms* **12** (2023), no. 2, Art. 218, 15 pp.
[12] H. M. Srivastava, F. A. Shah, W. Z. Lone, Quadratic-phase wave-packet transform in $L^2(\mathbb{R})$, *Symmetry* **14** (2022), no. 10, Art. 2018.
[13] W. Z. Lone, F. A. Shah, Shift-invariant spaces and dynamical sampling in quadratic-phase Fourier domains, *Optik* **260** (2022), Art. 169063.
[14] M. Kumar, T. Pradhan, Quadratic-phase Fourier transform of tempered distributions and pseudo-differential operators, *Integral Transforms Spec. Funct.* **33** (2022), no. 6, 449–465.
[15] C. Mateo, J. A. Talavera, Short-time Fourier transform with the window size fixed in the frequency domain (STFT-FD): implementation, *SoftwareX* **8** (2018), 5–8.
[16] R. G. Baraniuk, P. Flandrin, A. J. E. M. Janssen, O. J. J. Michel, Measuring time–frequency information content using the Rényi entropies, *IEEE Trans. Inform. Theory* **47** (2001), no. 4, 1391–1409.
[17] B. Boashash, Estimating and interpreting the instantaneous frequency of a signal, *Proc. IEEE* **80** (1992), no. 4, 520–538 and 540–568.
[18] I. Daubechies, The wavelet transform, time–frequency localization and signal analysis, *IEEE Trans. Inform. Theory* **36** (1990), no. 5, 961–1005.
[19] E. Bedrosian, A product theorem for Hilbert transforms, *Proc. IEEE* **51** (1963), no. 5, 868–869.
[20] F. A. Shah, A. A. Teali, A. Y. Tantary, Special affine wavelet transform and the corresponding Poisson summation formula, *Int. J. Wavelets Multiresolut. Inf. Process.* **19** (2021), no. 2, Art. 2050042.

Department of Mathematics, South Campus, University of Kashmir, Jammu and Kashmir, India
E-mail address: msuok21@gmail.com

Department of Mathematics, South Campus, University of Kashmir, Jammu and Kashmir, India
E-mail address: fasha@uok.edu.in